Journal of Superconductivity and Novel Magnetism (2024) 37:1089–1100
https://doi.org/10.1007/s10948-024-06689-7

RESEARCH

Enhanced Ferromagnetism in Nano-sized $Sn_{0.85}Co_{0.10}Fe_{0.03}Mn_{0.02}O_2$ Dilute Magnetic Semiconductor Synthesised by Sol–Gel Method

Renu Rajan[1] · R. Ezhil Vizhi[1]

Received: 29 November 2023 / Accepted: 2 January 2024 / Published online: 12 January 2024

Abstract
Co-Fe–Mn co-doped SnO_2 nanoparticles have been effectively synthesised by sol–gel method. To explore the effect of co-doping in instigating room-temperature ferromagnetism in SnO_2 nanocrystals, the structural, optical and magnetic behaviours of $Sn_{0.85}Co_{0.10}Fe_{0.03}Mn_{0.02}O_2$ nanoparticles were examined. Also, the oxidation states of dopants were evaluated using XPS analysis. XRD data exhibited pure SnO_2 phase, revealing the effectiveness of the method of synthesis in substituting the dopant ions into Sn sites. The average crystallite size of the synthesised sample was calculated to be 21 nm. SEM–EDX and HRTEM-SAED revealed the surface morphology, elemental composition, lattice plane and the polycrystalline nature of the nanoparticles. Diffuse reflectance spectroscopy data illustrated a decrease in bandgap compared to bulk SnO_2 due to the effect of dopants. FTIR spectrum disclosed the prominent peaks corresponding to SnO_2. The occurrence of room-temperature ferromagnetism in the prescribed sample has been validated from the magnetic hysteresis plotted using VSM data analysis. The analysis of all the abovementioned characterisations revealed the incorporation of dopants into SnO_2 host material. The emergence of magnetism in the sample depends mainly on the distribution of vacancy defects and nano-size of the sample, in addition to the surface diffusion of magnetic dopant ions into the SnO_2 lattice.

Keywords Oxide materials · Semiconductors · Nanostructured materials · Sol–gel processes · Magnetic measurements · X-Ray diffraction

1 Introduction

For more than two decades, the exploration of compounds that combine the features of both semiconductors and ferromagnets has developed into a significant area in materials science. Room-temperature ferromagnetism in diluted magnetic semiconductors (DMSs) and diluted magnetic oxides (DMOs) has grown into a dominant branch in this area. The presence of ferromagnetism above room temperature has been observed in a number of transition metal (TM) doped DMSs [1] and even in nanoparticles without minute traits of TM impurities [2]. However, in spite of frequent research on the origin of ferromagnetic behaviour in DMSs and control of spin in these systems, this area has become one of the most debatable topics for investigation in the field of materials science these days. A number of synthesis methods as well as theories which explain the magnetic origin in these architectures are in discussion right now [3–6]. In most of these studies, the cations of DMSs are to a certain extent replaced with the dopant TM ions to bring about ferromagnetism above room temperature. Since most of the TM dopants are ferromagnetic, these TM substitutions generate confusion on the origin of ferromagnetism in these semiconductors, which bring about much difficulty in the development of realistic DMS materials and device applications [7]. A detailed and precise understanding and investigation on room-temperature ferromagnetism in wide-bandgap DMSs has now emerged as one of the main challenges in recent field of magnetism [4, 8, 9]. From our understanding, the emergence of ferromagnetic nanoparticles can be manipulated by the various synthesis procedures and co-doping. There are certain cases which show ferromagnetism in undoped and non-TM doped DMOs which supports the intrinsic origin of ferromagnetism due to vacancy defects and nanometric size of the sample [2]. It is already understood that particles in nanodimension can disclose peculiar properties in contrast with their bulk

✉ R. Ezhil Vizhi
rezhilvizhi@vit.ac.in

[1] Materials Research Laboratory, Centre for Functional Materials, Vellore Institute of Technology, Vellore, Tamil Nadu, India

counterparts usually due to the huge difference in surface-to-volume ratio [10, 11]. However, the possibility of the role of impurity phases and TM segregates in the interfaces has been specified in some of the researches [12, 13]. At the same time, carrier-dependent ferromagnetic origin as well as the reliance on the TM or rare earth dopant and its concentration are also used to argue as the reason for ferromagnetism in many of the DMS systems [12, 14]. It is now a necessity to perceive the effect of dopant ions in the host matrix. Investigating on the structure and magnetic behaviour correlation is one of the best methods to confirm the intrinsic property of ferromagnetic behaviour and to control the favourable conditions that give rise to high Tc ferromagnetism in DMSs for realistic applications. Considering these factors, we have attempted for a detailed investigation on the structural and magnetic properties of SnO_2 nanoparticles when co-doped with Co, Fe and Mn transition metals. We have adopted a sol–gel-based synthesis procedure which is effective in producing nanodimensional particle samples which also serve as an uncomplicated method for nanoparticle synthesis [15]. In comparison with our previous works, the present study shows a comparatively enhanced ferromagnetic behaviour in SnO_2 nanoparticles when co-doped with Co, Fe and Mn ions [2, 16, 17]. The characteristic analyses done in the present work is compared with that of pure SnO_2 nanoparticles that was analysed in our previous work already reported [2].

2 Experimental

2.1 Material Preparation

Tin(IV) chloride pentahydrate ($SnCl_4{\cdot}5H_2O$) was purchased from Sigma-Aldrich. Cobalt(II) nitrate hexahydrate ($Co(NO_3)_2{\cdot}6H_2O$), iron(III) nitrate nonahydrate ($Fe(NO_3)_3{\cdot}9H_2O$), manganese dichloride tetrahydrate ($MnCl_2{\cdot}4H_2O$), citric acid anhydrous and ammonia solution were bought from Merck, Germany. All reagents used during the synthesis procedure were analytically pure and used without any additional purification. The Co-Fe–Mn co-doped SnO_2 nanoparticles were synthesised by sol–gel-based method of synthesis. $SnCl_4{\cdot}5H_2O$ was used as the source of tin and $Co(NO_3)_2{\cdot}6H_2O$, $Fe(NO_3)_3{\cdot}9H_2O$ and $MnCl_2{\cdot}4H_2O$ were used for cobalt, iron and manganese sources, respectively. A stoichiometric amount of citric acid was added to 85% of the weight for 1 M of $SnCl_4{\cdot}5H_2O$, 10% of the weight for 1 M of $Co(NO_3)_2{\cdot}6H_2O$, 3% of the weight for 1 M of $Fe(NO_3)_3{\cdot}9H_2O$ and 2% of the weight for 1 M of $MnCl_2{\cdot}4H_2O$, to obtain 0.85 composition of Sn, 0.10 composition of Co, 0.03 composition of Fe and 0.02 composition of Mn, in the synthesised $Sn_{0.85}Co_{0.10}Fe_{0.03}Mn_{0.02}O_2$ sample. Citric acid acts as a chelating agent in sol–gel method. An adequate quantity of ammonia solution was added drop wise to this solution under constant stirring in a magnetic stirrer until the pH retained in the range of 8–9. The addition of ammonia solution modifies pH and enhances cation binding to the citrate. The solution was continuously stirred for 3 h. Afterwards, the temperature in the stirrer was increased for the gel formation. The resultant dry gel was heated in an oven at 200 °C for 15 min. The black ash obtained was annealed at 600 °C for 5 h for the phase formation of pure SnO_2. Once cooled down to room temperature, the dark grey final product obtained was given for characterisation studies after proper grinding in a mortar.

2.2 Characterisations

Thermogravimetric analysis (TGA) along with differential scanning calorimetry (DSC) analysis of the as-prepared dry gel was carried out on a TGA operator (SDT Q600 V20.9 Build 20) from room temperature to 800 °C at a heating rate of 20 °C/min. The phase identification of the annealed powder was carried out by a Bruker D8 Advance powder X-ray diffractometer using Cu Kα radiation ($\lambda = 1.5406$ Å). The crystallite size, lattice parameter values and structure of the sample were calculated from the X-ray diffraction (XRD) data obtained. The particle morphology and local crystallographic structure were studied using a Jeol/JEM 2100 high-resolution transmission electron microscope (HRTEM) with 200 kV of accelerating voltage. Selected area electron diffraction (SAED) pattern obtained gave information about d-spacing and the crystallinity of the sample. The morphology of the samples were also analysed by SEM–EDX using Carl Zeiss EVO/18 and the chemical compositions were analysed by energy-dispersive X-ray spectroscopy (EDX) equipped with scanning electron microscope (SEM). ULVAC-PHI5000 Version Probe III was used to perform X-ray photoelectron spectroscopy (XPS) studies. XPS analysis provided elemental composition and electronic states of the elements within the sample. Optical properties of the prepared nanoparticles were characterised using a JASCO V-670 UV–Vis spectrophotometer. The presence of chemical bonding in the co-doped SnO_2 nanocrystals was studied using a Shimadzu IR Affinity Fourier-transform infrared spectrophotometer. The magnetic studies were carried out at room temperature by means of a Lakeshore VSM 7410 vibrating sample magnetometer with a maximum applied field of ± 15 kOe. All the characterisation analyses are compared with pure SnO_2 nanoparticles synthesised and reported in our previous work [2].

3 Results and Discussion

3.1 Thermal Characterisations

The TGA/DSC analysis has been carried out to interpret the process of decomposition occurring in Co-Fe–Mn doped SnO_2 nanoparticles (Fig. 1). $Sn_{0.85}Co_{0.10}Fe_{0.03}Mn_{0.02}O_2$

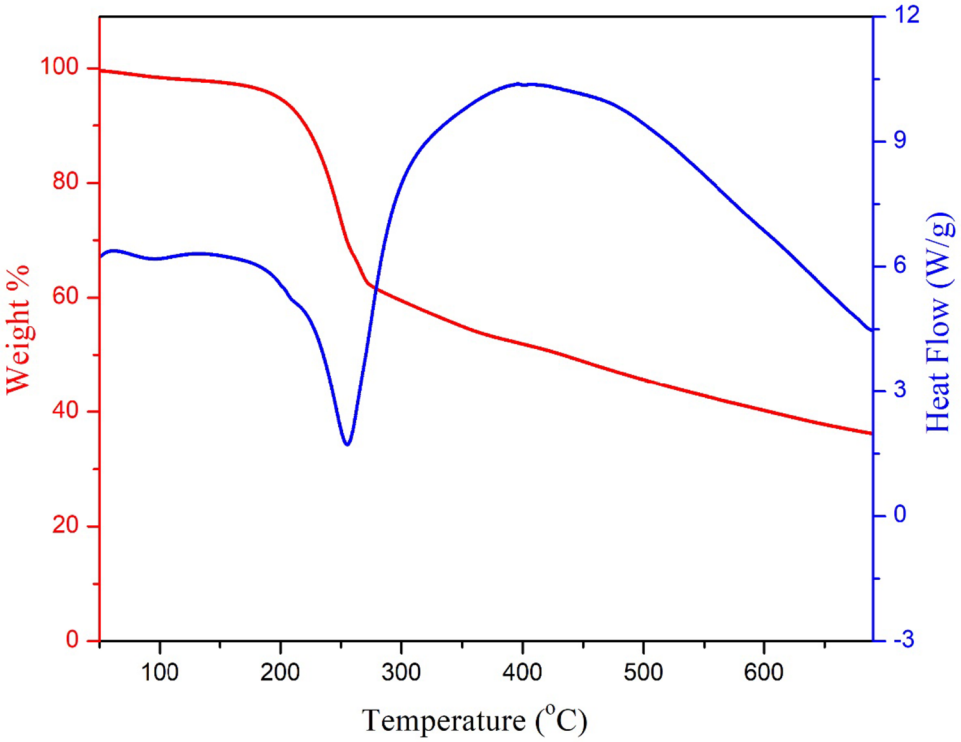

Fig. 1 TGA/DSC curve of Co-Fe–Mn co-doped SnO_2 nanoparticles

sample exhibited single-step decomposition behaviour. The endothermic peak in the DSC at around 250 °C was accompanied by a significant weight loss of about 40% in TGA due to the melting of some organic compounds along with decomposition to the SnO_2 phase. The presence of organic compounds can be due to the existence of citric acid that was added during the synthesis procedure [17]. The baseline shift following the endothermic peak corresponds to the volatilisation of residual organic compounds present in the sample.

3.2 Structure and Morphology

The phase identification, crystal structure, crystallite size and lattice constants of the $Sn_{0.85}Co_{0.10}Fe_{0.03}Mn_{0.02}O_2$ sample was computed using X-ray XRD data analysis [18]. All the peaks in the XRD pattern (Fig. 2) and the calculated lattice parameters match readily with tetragonal rutile phase of standard JCPDS No. 00–041-1445 of SnO_2. There were no other secondary peaks associated to the crystallised dopants or oxides of cobalt, iron or manganese in the diffraction pattern, which indicates that the dopant ions entirely incorporated into the SnO_2 lattice. The average crystallite size (D) of the sample (in nm) was calculated by applying the Scherrer equation [19]:

$$D = \frac{0.9\lambda}{\beta\cos\theta}$$

where λ, β and θ are the X-ray wavelength (1.54056 Å), full width at half maximum (FWHM) and the Bragg diffraction angle, respectively.

The average crystallite size calculated was 21 nm and lattice constants were $a = b = 4.735$ Å and $c = 3.182$ Å. It is obvious that even though the lattice parameters are slightly affected by the dopants, the crystal structure remains tetragonal. The lattice parameters show a negligible reduction compared to pure SnO_2 ($a = b = 4.742$ Å and $c = 3.188$ Å) [2].

Tin atoms are octahedrally coordinated in SnO_2 lattice. The reliable ionic states of Co, Fe and Mn are to be taken into account while considering the substitution of dopants. Foremost, the ionic radius of Sn^{4+} in octahedral coordination is 0.69 Å. So, the most possible ionic state of cobalt in octahedral coordination will be Co^{2+} which is having an ionic radius of 0.65 Å (comparable to the ionic radius of tin). Similarly, Fe^{3+} in octahedral coordination is the most viable ionic state of iron since its ionic radius is 0.645 Å. Manganese is the other dopant which is having the least concentration. While considering the ionic states of manganese in octahedral coordination, the most reliable will be Mn^{3+} with 0.645 Å as its ionic radius. However, the possibility of Mn^{4+} in octahedral coordination with 0.53 Å ionic radius cannot be completely omitted because of its less concentration and the minute reduction in lattice parameters with substitution of dopants. These substitutions infringe the charge balance. So, it can be anticipated that the charge neutrality might give rise to oxygen vacancies surrounding the substituted

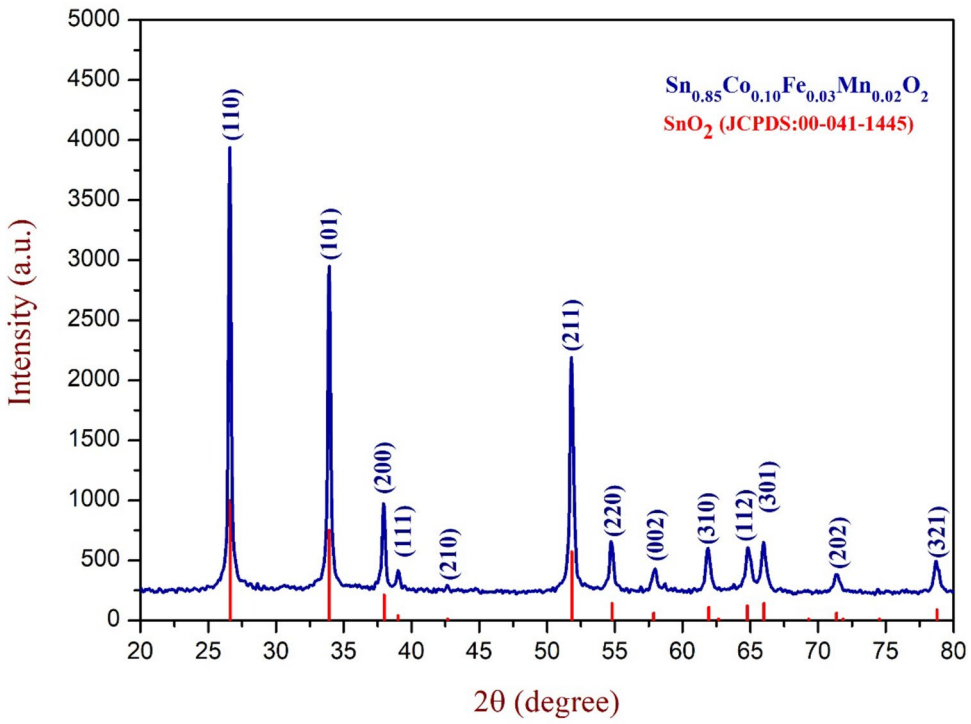

Fig. 2 X-Ray diffraction pattern of $Sn_{0.85}Co_{0.10}Fe_{0.03}Mn_{0.02}O_2$ nanocrystals annealed at 600 °C

ions [20]. As suggested by Kramers, this results in indirect ferromagnetic coupling of magnetic cations through intermediate oxygen anions [21, 22].

Williamson–Hall (W–H) method was considered to determine the microstrain originated due to Co-Fe–Mn substitution in SnO_2 lattice. W–H plot gives the relation between crystallite size and strain-induced broadening of the X-ray diffraction peak based on the following equation:

$$\beta\cos\theta = \frac{K\lambda}{D} + 4\varepsilon\sin\theta$$

where β is the strain-induced broadening and ε is the microstrain. In this concept, the induced strain is considered to be uniform in all the crystallographic directions. To deduce the induced strain, $\beta \cos \theta$ is plotted on y-axis against 4 sin θ on x-axis as illustrated in Fig. 3. The slope of the linear fit gives the microstrain corresponding to the doped SnO_2 sample which is equal to 6.46×10^{-3}. The relatively high value of microstrain will be possibly due to the defects and stress originated due to the variations in ionic radii of dopants compared to the ionic radii of Sn^{4+} in octahedral coordination.

TEM and HRTEM images along with the corresponding SAED pattern of $Sn_{0.85}Co_{0.10}Fe_{0.03}Mn_{0.02}O_2$ nanoparticles are shown in Fig. 4. TEM image displays non-uniform particle sizes with an average size of 18 nm. Lattice fringes seen in HRTEM show interplanar spacing of 0.24 nm. It corresponds to (200) plane of the lattice. The SAED pattern confirms the polycrystalline nature of the sample. The two SAED rings marked are assigned to (111) and (110) lattice planes of SnO_2. SEM–EDX obtained are shown in Fig. 5. The sample mostly contains clusters of small agglomerated particles with a non-uniform surface morphology. The EDX analysis confirmed the presence of Sn, O, Co, Fe and Mn elements in the doped sample. The weight percentages of the dopants were observed to be close to stoichiometric concentration chosen during the synthesis procedure.

3.3 X-Ray Photoelectron Spectroscopy

The XPS core level spectra and survey scan spectrum of $Sn_{0.85}Co_{0.10}Fe_{0.03}Mn_{0.02}O_2$ nanocrystals are illustrated in Fig. 6. The binding energies of Sn $3d_{5/2}$ and Sn $3d_{3/2}$ are 486.52 eV and 494.99 eV, respectively, indicating Sn^{4+} ions in the sample [23]. The binding energy of Sn $3d_{5/2}$ and other two peaks observed at 25.90 eV and 715.8 eV corresponding to Sn $4d_{5/2}$ and Sn $3p_{3/2}$, respectively, implies the chemical state of SnO_2 [24]. The single intense peak at 530.94 eV corresponds to O 1 s of lattice oxygen in SnO_2. The peaks at 781.20 eV and 796.94 eV correspond to Co $2p_{3/2}$ and Co $2p_{1/2}$, respectively. The satellite peak of Co 2p at 786.87 eV confirms the Co^{2+} ionic state of cobalt [25]. The peaks of Co 3 s and Co 3p at 102.6 eV and 61.8 eV also indicate Co^{2+} oxidation state. Fe $2p_{3/2}$ peak at 708.04 eV and satellite peak of Fe $2p_{1/2}$ at 729.9 eV correspond to Fe^{3+} state. Fe 3 s at 95 eV also confirms the 3 + state of Fe ion [25, 26]. Now, considering the binding

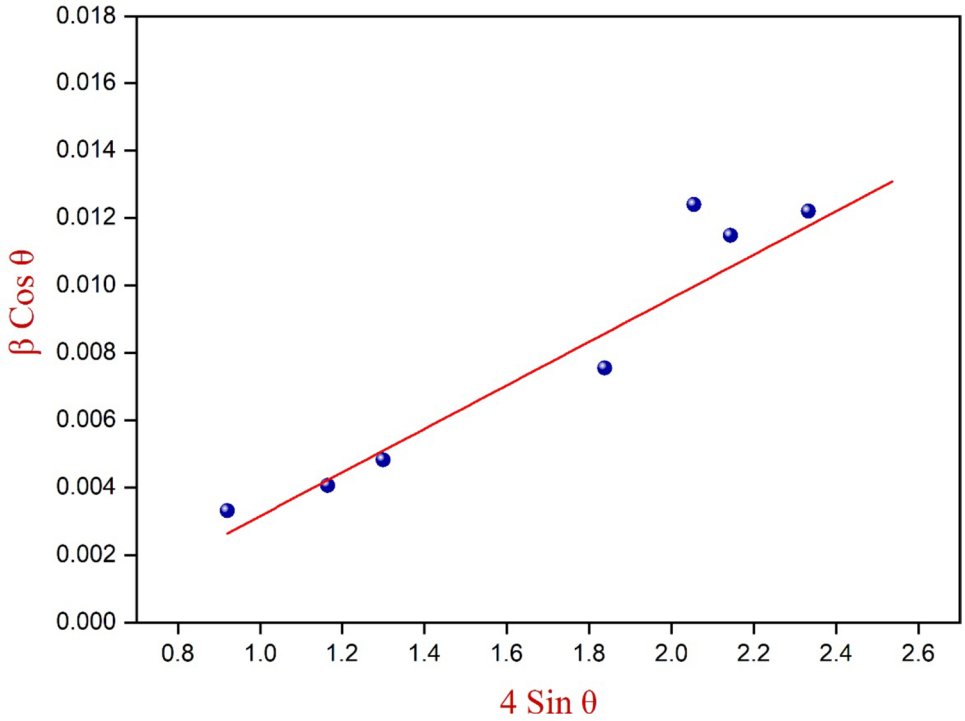

Fig. 3 W–H plot of $Sn_{0.85}Co_{0.10}Fe_{0.03}Mn_{0.02}O_2$ nanoparticles

energies of Mn peaks at 642.8 eV and 653.1 eV indicates Mn $2p_{3/2}$ and Mn $2p_{1/2}$, respectively. This peak splitting ($\Delta E = 10.3$ eV) represents Mn^{3+} oxidation state. Mn 3 s peak also distinguishes the oxidation state of Mn which is found to be at 88.5 eV. It represents Mn^{4+} state of Mn. So, it can be confirmed that Mn exists as the mixed state of Mn^{3+} and Mn^{4+} in the $Sn_{0.85}Co_{0.10}Fe_{0.03}Mn_{0.02}O_2$ sample [23, 27]. XPS spectra analysis confirms the inference that we obtained from XRD analysis based on the ionic radii of the corresponding dopants.

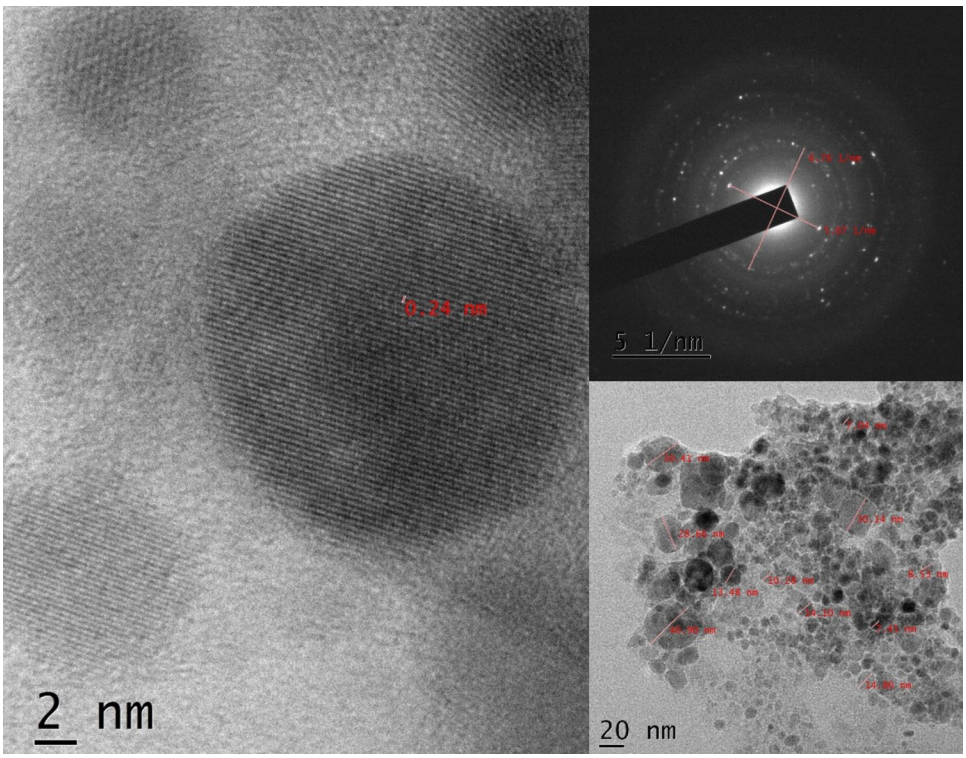

Fig. 4 HRTEM, TEM and SAED pattern of $Sn_{0.85}Co_{0.10}Fe_{0.03}Mn_{0.02}O_2$ nanoparticles

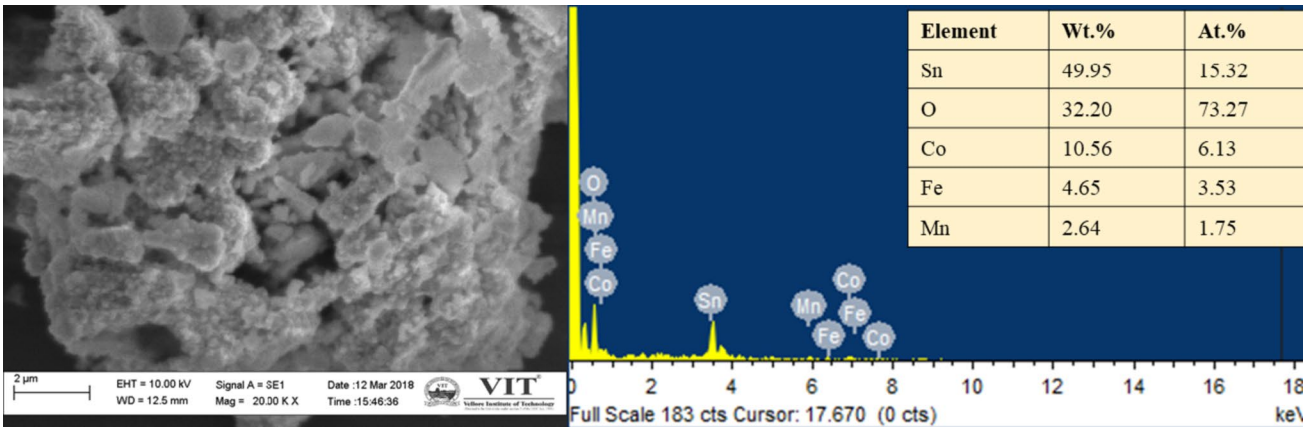

Element	Wt.%	At.%
Sn	49.95	15.32
O	32.20	73.27
Co	10.56	6.13
Fe	4.65	3.53
Mn	2.64	1.75

Fig. 5 SEM and EDX spectrum of $Sn_{0.85}Co_{0.10}Fe_{0.03}Mn_{0.02}O_2$ nanoparticles

3.4 Optical Measurements

The optical properties of $Sn_{0.85}Co_{0.10}Fe_{0.03}Mn_{0.02}O_2$ nanoparticles were analysed by UV–visible diffuse reflectance spectroscopy (DRS). The sample showed an absorption edge close to 300 nm (Fig. 7) owing to comparatively large exciton binding energy of SnO_2 [28]. The replacement of many of the Sn ions by the dopant ions in SnO_2 nanoparticles showed an increase in the range of absorption throughout the spectrum. The broad absorption in the visible region after doping is mainly due to the presence of oxygen vacancy defects that creates an intermediate state in the bandgap, which makes the absorption easier in the visible region. The dopants are p-type since the valence electrons of all dopants are less than 4 which help to form free holes within the semiconductor. In a p-type material, there is an increase in the

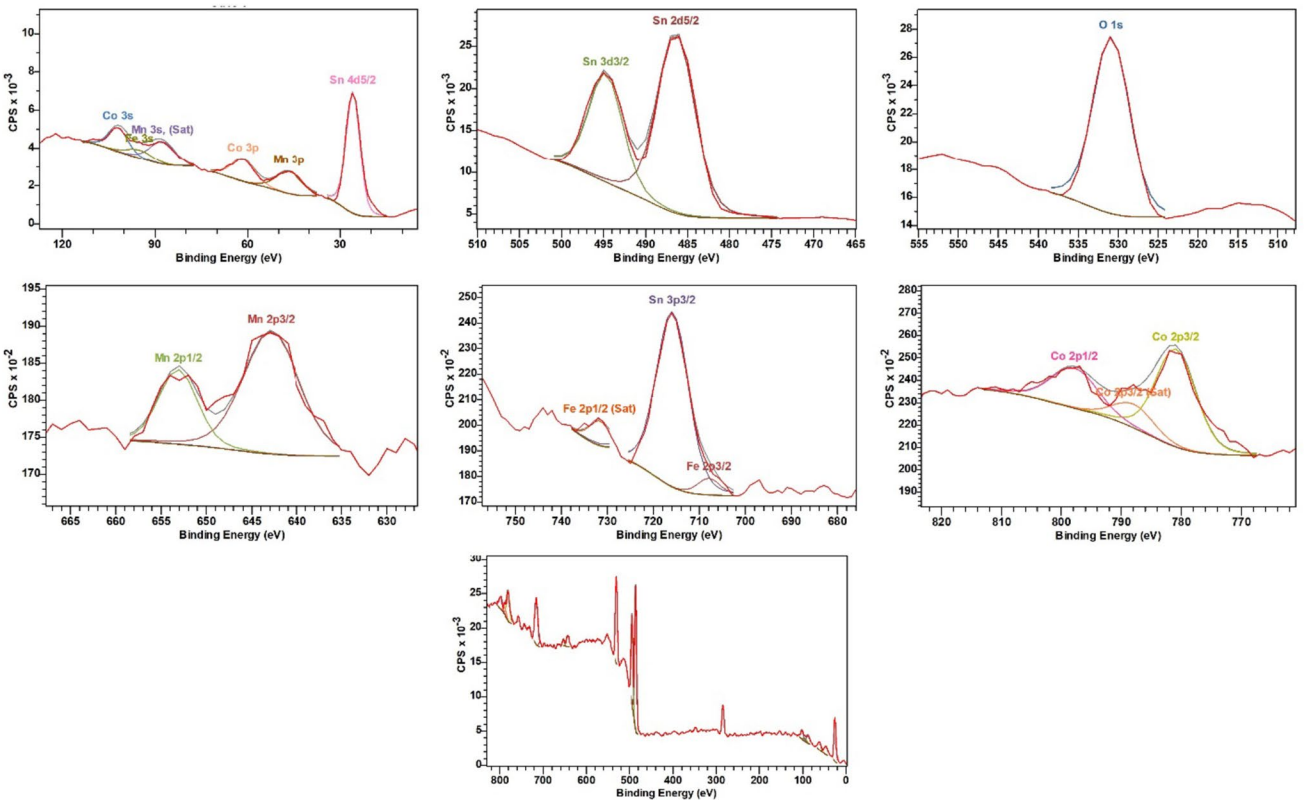

Fig. 6 XPS core level spectra and wide scan spectrum of $Sn_{0.85}Co_{0.10}Fe_{0.03}Mn_{0.02}O_2$ annealed at 600 °C

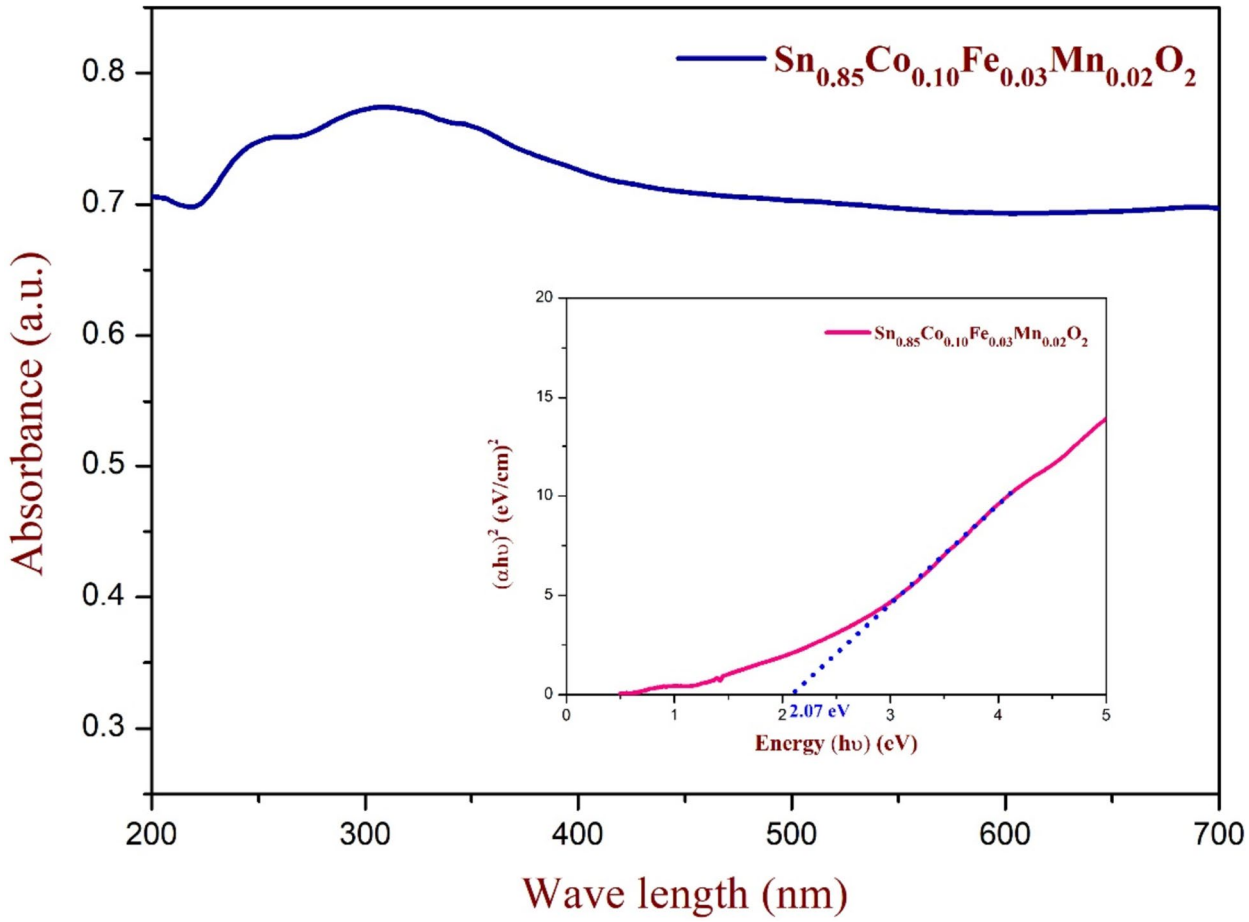

Fig. 7 UV absorption spectra and direct band gap (in inset) through extrapolation of the linear range of $(\alpha h\upsilon)^2$ for $y=0$, for $Sn_{0.85}Co_{0.10}Fe_{0.03}Mn_{0.02}O_2$ nanoparticles

density of unfilled states; therefore, more electrons can be accommodated at lower energy states. It is observed experimentally that shrinkage of the band gap occurs when the dopants' concentration is particularly high. The direct band gap energy (2.07 eV) of the sample is shown in the inset of Fig. 7. A remarkable reduction in the band gap was observed with doping when compared to pure SnO_2 [2]. The band gap is reduced due to the defect states produced by dopants in the band gap of SnO_2. Dopants' radii have also influenced the band gap reduction because larger ionic radii would result in a larger band gap.

3.5 Fourier-Transform Infrared Spectroscopy

The Fourier-transform infrared spectroscopy (FTIR) spectra (Fig. 8) revealed the main IR features of SnO_2 at 455 cm^{-1} and 603 cm^{-1} assigned to O–Sn–O and Sn–O stretching vibrations, respectively [29]. No peaks corresponding to OH vibrations due to the adsorption of atmospheric water were observed. The existence of these peaks credited to Sn–O bond vibrations confirm the formation of SnO_2 phase. No peaks corresponding to the clusters of dopants were observed. The FTIR spectrum was observed to be slightly affected by doping. It is found that the O–Sn–O stretching vibration frequency shows a small red shift compared to pure SnO_2 [2] due to the substitution of dopants in Sn sites. However, there is not much change in the intensity of the peaks compared to pure sample which indicates that the structure of the sample is not altered by doping.

3.6 Magnetic Characterisation

The room-temperature magnetic nature of the $Sn_{0.85}Co_{0.10}Fe_{0.03}Mn_{0.02}O_2$ sample for an externally applied magnetic field of ± 15 kOe illustrated in Fig. 9 was observed to be ferromagnetic. The existence of polycrystalline nature of the sample confirmed from TEM-SAED pattern instigate enormous defect centres comprising vacancies as well as dislocations in the sample, which also plays an important role in the magnetic properties [30]. This possibility of defects can also be ascribed to the chemical synthesis method. The decrease in the coordination number in the

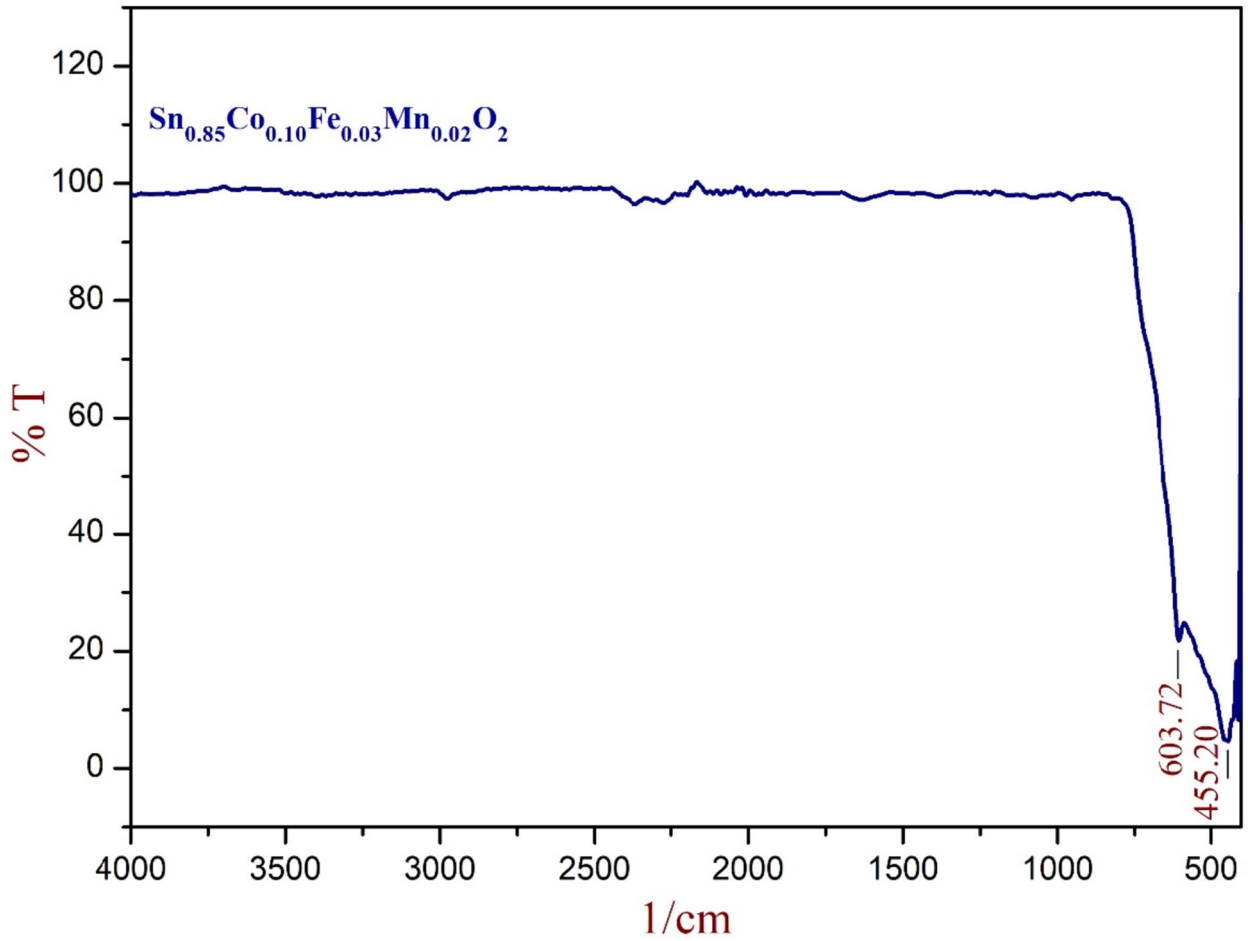

Fig. 8 FTIR spectra of $Sn_{0.85}Co_{0.10}Fe_{0.03}Mn_{0.02}O_2$ nanoparticles

nano-size will also promote ferromagnetic characteristics. Due to the dramatically increased surface-to-volume ratio in these porous nanoparticles, magnetic properties remarkably change compared to that of the bulk material with the same chemical composition. Due to the reduced coordination number, there is a decrease in the overlap of the nearby atomic orbitals that makes it difficult for the electrons to hop between the sites, which in turn lessens the kinetic energy and thereby reducing the band gap [31]. This will lead to the sharper density of states. This intensification of local density of states reinforce the inclination to magnetism [32]. So, the magnetic moment per atom increases with the decrease in coordination number. Also, the effect of vacancies on the nearest-neighbour magnetic atoms also tends to enhance its magnetic moments.

From our investigation, it can be presumed that the dopant ions also play an important role in the observed magnetic behaviour. To be precise, the major contribution to ferromagnetism in this sample is the dopants itself, even though the contribution due to defects cannot be omitted. A close inspection on the hysteresis of the sample reveals that there is a small paramagnetic contribution which can be due to the ionic states of manganese analysed from XPS data. This is because, even though ferromagnetic, the saturation magnetisation observed is not attaining the saturation. The ionic states of manganese observed from XPS are paramagnetic. It characterises an enhancement in magnetism with increase in applied external magnetic field. The major ferromagnetic contribution can be due to the other two dopants (Co and Fe) which are ferromagnetic. However, the possibility of intrinsic ferromagnetism in this sample cannot be completely ruled out because there were no secondary phases (due to clusters or oxides of dopants) from the structural analyses performed for the prescribed sample. From our research, the electro-neutrality should generate a considerable number of oxygen vacancies due to the replacement of Sn^{4+} ions by dopant ions (Co^{2+}, Fe^{3+} and Mn^{3+}) in the sample. These vacancies will be surrounding the cations of dopants. The localised ions of the dopants will interact with the free carriers bound to the oxygen vacancies which support to develop magnetic polarisation [20].

The existence of ferromagnetism in DMS materials has been explained by a number of theories, but the exact cause

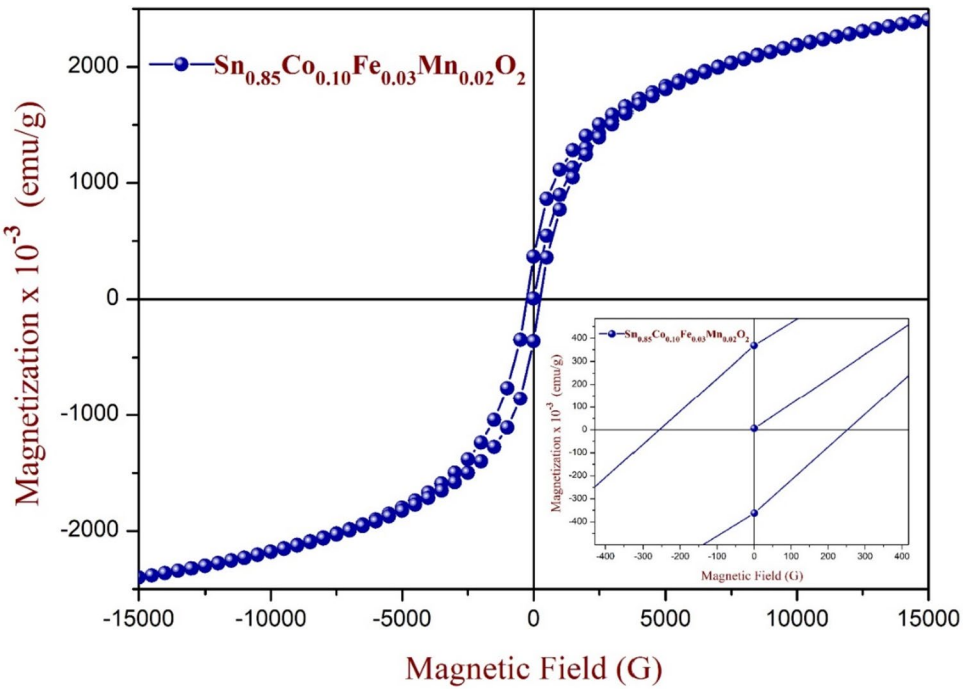

Fig. 9 Magnetic hysteresis loop of $Sn_{0.85}Co_{0.10}Fe_{0.03}Mn_{0.02}O_2$ nanoparticles

of RTFM is still unresolved. The most commonly proposed theories to explain ferromagnetism in DMSs are Zener Model, Ruderman–Kittel–Kasuya–Yosida (RKKY) model, Mean-Field Zener Model, the Double Exchange Model and the Bound Magnetic Polaron model. Among these models, the present work explains BMP model as the reason for the observed ferromagnetic ordering in the synthesised nanoparticles. BMP model proposes a long-range ferromagnetic condition resulting from the overlapping of two nearby magnetic polarons. When the polaron size is nearly equal to the sample size, the ferromagnetic transition takes place. Coey postulated that the donor electrons entrapped by the oxygen vacancy, which have a tendency to form BMPs in their hydrogenic orbits, mediate the ferromagnetic exchange pairing of transition metal ions in the n-type dilute magnetic oxides [4, 33]. The only possible electrons unfilled in 3d orbitals, for a $3d^5$ ion like Fe^{3+} or Mn^{2+}, are spin-down electrons. The donor electron is therefore in a spin-down state, and ferromagnetic coupling between two magnetic impurities in the same donor orbital is the most feasible [4, 34]. When the 3d shell is less than half full, the coupling between both the donor electron as well as the cation will typically be ferromagnetic, and when it is half full or more, it will be antiferromagnetic. In any scenario, there will be ferromagnetic coupling involving two similar impurities that are present in the same donor orbital. The hydrogenic orbitals connected to the randomly located defects overlap as the donor defect concentration rises, forming a spin-split donor impurity band [4]. According to the discussions of the BMP model, the ferromagnetic characteristics of dilute magnetic oxides are greatly affected by defects. The shallow donors created by the oxygen vacancy defects in the BMP model strongly stabilise the ferromagnetic ground state. Errico et al. [35] proposed that oxygen vacancies in an acceptable percentage can give the required carriers to stabilise the ferromagnetic state. Since this model is also explained based on the defects such as oxygen vacancies or other interstitial defects, BMP model can be considered as the best possible model for explaining RTFM in O-DMSs. No other models explain ferromagnetism, on the basis of vacancy defects, where the present work reports the occurrence of RTFM due to oxygen vacancy defects in doped SnO_2 which can only be explained with the help of the BMP model.

To obtain a more detailed analysis of each dopant's specific contribution to the properties of SnO_2 nanoparticles, some of our previous works are considered. Co doping in SnO_2 nanoparticles enhanced with the increase in Co concentration. However, Co concentration increased beyond a limit will give rise to secondary peaks [17]. So, the dopant concentration should be kept very low while synthesising DMS materials. Introduction of Fe ions to the Co-doped SnO_2 will further enhance the magnetic behaviour due to the ionic states of these magnetic dopants [36]. The half-filled 3d orbitals of these Co^{2+} and Fe^{3+} ions result in enhanced magnetism in these materials. As explained by the BMP model, the overlapping of two nearby polarons results in magnetism. The donor electrons will be entrapped in the oxygen vacancy, which have a tendency to form BMPs in their hydrogenic orbits which mediate the ferromagnetic exchange pairing of transition metal ions in the DMS oxides.

Furthermore, Mn^{3+} and Mn^{4+} oxidation states are more paramagnetic compared to other dopants due to the distribution of electrons in 3d orbitals of these ions.

The empirical results reported herein should be considered in the light of some limitations. In general, a number of factors contribute to the complexity of creating DMSs for practical gadgets in electronics. The fundamental limitation results from the commercial use of silicon (Si) and gallium arsenide (GaAs), both of which are intrinsically nonmagnetic. Furthermore, the huge energy difference between the two possible spin orientations (up and down) in magnetic materials means that manipulating them requires an excessively high magnetic field, which further restricts their commercialisation [37]. In the present study, the primary cause of magnetisation in these DMS materials was confirmed to be due to the vacancy defects created in these systems. Formation of vacancy defects largely depends on the synthesis procedure in addition to dopant ions among the various factors. It is challenging to precisely manipulate or control the defects in these crystal structures. That is the reason for the varying magnetisations that have been reported for the same host material doped with the very same concentration of identical dopants [37, 38]. While the magnetic behaviour of these materials can be enhanced by several kinds of dopants, the behaviour of individual dopant ions in an externally applied magnetic field will differ. This is because each magnetic material has a different direction of spin of electrons within the orbitals, which results in the magnetic behaviour of the material. Even though RTFM was observed in the present study, researches show that the enhancement of magnetisation for operational temperatures is challenging in these DMS materials. As a result, for commercial applications, a thorough investigation of magnetic ions and its behaviour in these host semiconductor material is required.

Considering the future research directions, oxide semiconductors are superior to non-oxide semiconductors in several ways. They are appropriate for short-wavelength applications due to their wide band gap. They are inexpensive, durable, safe for the environment and easily grown at low temperatures—even on a plastic substrate. Furthermore, high p–d exchange coupling between band carriers and localised spins is anticipated to result from strong oxygen electronegativity, which is an essential requirement for DMS [37, 39]. So, other oxide-based semiconductors can be considered for future research. A real DMS has a small number of magnetic impurities, like TMs or rare earths, randomly doped into the host semiconductor. In the semiconductors, this results in the coexistence of itinerant free carriers (either electrons or holes) and localised spins of the magnetic ions. The localised spins of the magnetic impurities interact with one another in the presence of free carriers, causing the host material to acquire magnetic properties. However, the exact reason for magnetisation has to be analysed. This is because impurities, magnetic clusters, interstitial and vacancy defects, oxidation state of magnetic ions etc. are also responsible for the magnetism in these systems. So, an in-depth study on magnetism is required.

Moreover, ferromagnetic DMS must be operational at room temperature in order to be implemented in practical applications. To attain room-temperature ferromagnetism in these semiconductors, precise control over carrier doping and magnetic alloying is necessary. Once a better magnetisation is obtained above operational temperatures, various magnetic studies like temperature-dependent magnetisation, Curie temperature and magnetic susceptibility can be analysed for a detailed interpretation on magnetism. The nature of the exchange interaction between the free carriers and magnetic ions, or carrier-induced ferromagnetism in DMS depends upon their respective concentrations.

In fact, the goal of the present research aims to enhance room temperature ferromagnetism (RTFM) in order to create a new class of spintronic devices, including optical isolators, ultra-fast optical switches, magnetic sensors, spin valves, transistors and spin light-emitting diodes. These spintronic devices have the potential to be faster, more efficient, more stable and use less energy to flip a spin, among other benefits. It can definitely address two issues facing the computing industry: (1) removing the computer's waste heat and (2) increasing computing power without generating more heat [37, 40].

In electronics, magnetic random access memory (MRAM) chips and other storage devices can be fabricated using these materials. Due to its non-volatile memory, extremely fast operation and low power consumption, MRAM is superior than static RAM (SRAM) and dynamic RAM (DRAM) [41, 42]. All current memory devices could eventually be replaced by MRAM, which has the potential to become a universal solid-state memory. When MRAM is employed, standby power consumption is reduced, no disk drive booting occurs and eventually the computer system can be integrated on a single chip [43]. According to Datta and Das [44], a spin transistor is a magnetically sensitive transistor that uses the spin-up and spin-down states of electrons to function and store data. The spin transistor's primary benefit over existing semiconductor transistor technology is its ability to detect and modify electron spin states without the need for an electric current. As a consequence, the hardware devices become smaller and more sensitive. Solid-state storage devices that are affordable and non-volatile can be made using the spin transistor.

Compared to silicon chips and circuit elements now in use, spintronic devices are more compact, adaptable and durable. Information is stored into electron spins (up or down). Information is carried along a wire by the spins that are attached to mobile electrons, and read heads at a terminal read the data. Unlike charge-based data, which vanishes when electricity is cut off, spin allows them to save information even when it is

no longer powered. As the conduction electron spin orientations retain relatively for a long time, spintronic devices are especially useful for applications involving magnetic sensors and memory storage. There is less heat dissipation while the spin current flows. Spintronic devices are a means to accomplish device miniaturisation [44].

4 Conclusions

The analysis of all characterisations performed in our investigation reveal that the structural, morphological, optical and magnetic behaviour can be altered by the synthesis procedure. The tetragonal crystal structure, crystallite size < 25 nm, rough surface morphology, elemental composition, lattice planes and polycrystalline nature of the $Sn_{0.85}Co_{0.10}Fe_{0.03}Mn_{0.02}O_2$ samples were confirmed from the XRD, SEM–EDX and HRTEM-SAED pattern analysis. XPS data analysis confirmed the purity of the compound and oxidation states of each and every element present in the sample. UV–Vis spectroscopy analysis disclosed a reduced bandgap of the synthesised nanoparticle due to the effect of dopants. The chemical bonding corresponding to the host material was confirmed from FTIR spectrum analysis. The reduced coordination number due to nanodimension and vacancy defect gave rise to ferromagnetism in these nanoparticles. This will also result in reducing the bandgap due to the lower kinetic energy of electrons caused by the lesser possibility of electrons to hop between the sites. Magnetic studies also confirmed that ferromagnetism can be induced into SnO_2 nanocrystals by the incorporation of transition metal dopants. As conclusion, our research convey the effect of vacancy defects and influence of TM dopants on the magnetic behaviour of DMS materials. The nanofabrication method and the analysis of characterisations performed for our present work will be undoubtedly helpful for enhancing the magnetic behaviours of the ongoing and impending research in SnO_2 as well as in other oxide-based diluted magnetic semiconductor materials.

Acknowledgements The authors thank the management of Vellore Institute of Technology, Vellore, for their constant support and the characterisation facilities provided. The authors also thank SAIF, IIT Madras, for providing VSM measurements; STIC, CUSAT, for carrying out HRTEM/SAED and Nanotechnology Research Centre (NRC), SRMIST, for providing XPS analysis of the synthesised nanoparticles.

Author Contributions R.R: Conceptualization, Methodology, Data curation, Formal analysis, Writing – original draft, Resources, Investigation, Validation. R.E.V: Supervision, Writing - review & editing.

Funding No funding was received to assist with the preparation of this manuscript.

Data Availability No datasets were generated or analysed during the current study.

Declarations

Ethical Statement The authors declare that this manuscript complies with scientific ethical standards. There are no other persons who satisfied the criteria for authorship and are not listed. We further confirm that the order of authors listed in the manuscript has been approved by all of us. Furthermore, this article does not contain any studies involving human or animal participants.

Conflict of Interest The authors declare no competing interests.

References

1. Matsumoto, Y., Murakami, M., Shono, T., Hasegawa, T., Fukumura, T., Kawasaki, M., Ahmet, P., Chikyow, T., Koshihara, S., Koinuma, H.: Room-temperature ferromagnetism in transparent transition metal-doped titanium dioxide. Science(80-.) **80**(291), 854–856 (2001). https://doi.org/10.1126/science.1056186
2. Rajan, R., Vizhi, R.E.: Investigation of room-temperature ferromagnetism on pristine and non-ferromagnetic dopant-substituted SnO2 nanoparticles. J. Supercond. Nov. Magn. **30**, 3199–3206 (2017). https://doi.org/10.1007/s10948-017-4118-1
3. Dietl, T.: A ten-year perspective on dilute magnetic semiconductors and oxides. Nat. Mater. **9**, 965–974 (2010). https://doi.org/10.1038/nmat2898
4. Coey, J.M.D., Venkatesan, M., Fitzgerald, C.B.: Donor impurity band exchange in dilute ferromagnetic oxides. Nat. Mater. **4**, 173–179 (2005). https://doi.org/10.1038/nmat1310
5. Albanese, E., Leccese, M., Di Valentin, C., Pacchioni, G.: Magnetic properties of nitrogen-doped ZrO2: theoretical evidence of absence of room temperature ferromagnetism. Sci. Rep. **6**, 31435 (2016). https://doi.org/10.1038/srep31435
6. MacDonald, A.H., Schiffer, P., Samarth, N.: Ferromagnetic semiconductors: moving beyond (Ga, Mn)As. Nat. Mater. **4**, 195–202 (2005). https://doi.org/10.1038/nmat1325
7. Lee, J., Subramaniam, N.G., Agnieszka Kowalik, I., Nisar, J., Lee, J., Kwon, Y., Lee, J., Kang, T., Peng, X., Arvanitis, D., Ahuja, R.: Towards a new class of heavy ion doped magnetic semiconductors for room temperature applications. Sci. Rep. **5**, 17053 (2015). https://doi.org/10.1038/srep17053
8. Dietl, T.: Functional ferromagnets **2**, 4–6 (2003)
9. Kittilstved, K.R., Liu, W.K., Gamelin, D.R.: Electronic structure origins of polarity-dependent high-TC ferromagnetism in oxide-diluted magnetic semiconductors. Nat. Mater. **5**, 291–297 (2006). https://doi.org/10.1038/nmat1616
10. Aragón, F.H., Cohen, R., Coaquira, J.A.H., Barros, G.V., Hidalgo, P., Nagamine, L.C.C.M., Gouvêa, D.: Effects of particle size on the structural and hyperfine properties of tin dioxide nanoparticles. Hyperfine Interact. **202**, 73–79 (2011). https://doi.org/10.1007/s10751-011-0340-6
11. Dopants in nanocrystalline tin dioxide: Rumyantseva, M.N., Safonova, O. V., Boulova, M.N., Ryabova, L.I., Gas'kov, A.M. Russ. Chem. Bull. **52**, 1217–1238 (2003). https://doi.org/10.1023/A:1024916020690
12. Punnoose, A., Seehra, M.S., Park, W.K., Moodera, J.S.: On the room temperature ferromagnetism in Co-doped TiO2 films. J. Appl. Phys. **93**, 7867–7869 (2003). https://doi.org/10.1063/1.1556121
13. Park, J.H., Kim, M.G., Jang, H.M., Ryu, S., Kim, Y.M.: Co-metal clustering as the origin of ferromagnetism in Co-doped ZnO thin films. Appl. Phys. Lett. **84**, 1338 (2004). https://doi.org/10.1063/1.1650915
14. Philip, J., Punnoose, A., Kim, B.I., Reddy, K.M., Layne, S., Holmes, J.O., Satpati, B., LeClair, P.R., Santos, T.S., Moodera,

J.S.: Carrier-controlled ferromagnetism in transparent oxide semiconductors. Nat. Mater. **5**, 298–304 (2006). https://doi.org/10.1038/nmat1613
15. Punnoose, A., Hays, J., Gopal, V., Shutthanandan, V.: Room-temperature ferromagnetism in chemically synthesized Sn1−xCoxO2 powders. Appl. Phys. Lett. **85**, 1559–1561 (2004). https://doi.org/10.1063/1.1786633
16. Van Komen, C., Thurber, A., Reddy, K.M., Hays, J., Punnoose, A.: Structure–magnetic property relationship in transition metal (M=V, Cr, Mn, Fe Co, Ni) doped SnO2 nanoparticles. J. Appl. Phys. **103**, 07D141 (2008). https://doi.org/10.1063/1.2836797
17. Rajan, R., Vizhi, R.E.: Effect of Co3+ substitution on the structural, optical, and room-temperature magnetic properties of SnO2 nanoparticulates. J. Mater. Sci. Mater. Electron. **32**, 12716–12724 (2021). https://doi.org/10.1007/s10854-021-05906-6
18. Chikhale, L.P., Patil, J.Y., Rajgure, A.V., Shaikh, F.I., Mulla, I.S., Suryavanshi, S.S.: Co-precipitation synthesis of nanocrystalline SnO2: effect of Fe doping on structural, morphological and ethanol vapor response properties. Measurement **57**, 46–52 (2014). https://doi.org/10.1016/J.MEASUREMENT.2014.07.011
19. Muthukumaran, S., Gopalakrishnan, R.: Structural, optical, FTIR and photoluminescence properties of Zn0.96−xCo0.04CuxO (x=0.03, 0.04 and 0.05) nanopowders. Phys. B Condens. Matter. **407**, 3448–3456 (2012). https://doi.org/10.1016/J.PHYSB.2012.04.057
20. Nakai, I., Sasano, M., Inui, K., Korekawa, T., Ishijima, H., Katoh, H., Li, Y.J., Kurisu, M.: Oxygen vacancy and magnetism of a room temperature ferromagnet Co-doped TiO2. J. Korean Phys. Soc. **63**, 532–537 (2013). https://doi.org/10.3938/jkps.63.532
21. Kanamori, J.: Superexchange interaction and symmetry properties of electron orbitals. J. Phys. Chem. Solids **10**, 87–98 (1959). https://doi.org/10.1016/0022-3697(59)90061-7
22. Goodenough, J.B.: Theory of the role of covalence in the perovskite-type manganites [La, M (II)]MnO3. Phys. Rev. **100**, 564–573 (1955). https://doi.org/10.1103/PhysRev.100.564
23. Zhu, S., Chen, C., Li, Z.: Magnetic enhancement and magnetic signal tunability of (Mn, Co) co-doped SnO2 dilute magnetic semiconductor nanoparticles. J. Magn. Magn. Mater. **471**, 370–380 (2019). https://doi.org/10.1016/j.jmmm.2018.09.106
24. Lee, A.Y., Blakeslee, D.M., Powell, C.J., Rumble, J.R., Jr.: Development of the web-based NIST Xray Photoelectron Spectroscopy (XPS) Database. Data Sci. J. **1**, 1–12 (2002). https://doi.org/10.2481/dsj.1.1
25. Biesinger, M.C., Payne, B.P., Grosvenor, A.P., Lau, L.W.M., Gerson, A.R., Smart, R.S.C.: Resolving surface chemical states in XPS analysis of first row transition metals, oxides and hydroxides: Cr, Mn, Fe. Co and Ni. Appl. Surf. Sci. **257**, 2717–2730 (2011). https://doi.org/10.1016/j.apsusc.2010.10.051
26. Fu, Y., Sun, N., Feng, L., Wen, S., An, Y., Liu, J.: Local structure and magnetic properties of Fe-doped SnO 2 films. J. Alloys Compd. **698**, 863–867 (2017). https://doi.org/10.1016/j.jallcom.2016.12.297
27. Bilovol, V., Ferrari, S., Saccone, F.D., Pampillo, L.G.: Effect of the dopant on the structural and hyperfine parameters of Sn 0.95 M 0.05 O 2 nanoparticles (M: V, Mn, Fe, Co). Mater. Res. Express. **6**, 0850h6 (2019). https://doi.org/10.1088/2053-1591/ab29cc
28. Uddin, M.T., Nicolas, Y., Olivier, C., Toupance, T., Servant, L., Müller, M.M., Kleebe, H.-J., Ziegler, J., Jaegermann, W.: Nanostructured SnO 2 –ZnO heterojunction photocatalysts showing enhanced photocatalytic activity for the degradation of organic dyes. Inorg. Chem. **51**, 7764–7773 (2012). https://doi.org/10.1021/ic300794j
29. Kuantama, E., Han, D.-W., Sung, Y.-M., Song, J.-E., Han, C.-H.: Structure and thermal properties of transparent conductive nanoporous F:SnO2 films. Thin Solid Films **517**, 4211–4214 (2009). https://doi.org/10.1016/j.tsf.2009.02.044
30. Ma, J., Liu, C., Chen, K.: Assembling non-ferromagnetic materials to ferromagnetic architectures using metal-semiconductor interfaces. Sci. Rep. **6**, 34404 (2016). https://doi.org/10.1038/srep34404
31. Vaseashta, A., Mihailescu, I.N.: Functionalized nanoscale materials, devices and systems. Springer (2008)
32. Gemming, S. (Sibylle), Schreiber, M., Suck, J.B.: Materials for tomorrow: theory, experiments, and modelling. 194 (2007)
33. Coey, J.M.D.: High-temperature ferromagnetism in dilute magnetic oxides. J. Appl. Phys. **97**, 8–11 (2005). https://doi.org/10.1063/1.1849054
34. Coey, J.M.D., Douvalis, A.P., Fitzgerald, C.B., Venkatesan, M.: Ferromagnetism in Fe-doped SnO2 thin films. Appl. Phys. Lett. **84**, 1332–1334 (2004). https://doi.org/10.1063/1.1650041
35. Errico, L.A., Rentería, M., Weissmann, M.: Theoretical study of magnetism in transition-metal-doped TiO2 and TiO2−δ. Phys. Rev. B **72**, 184425 (2005). https://doi.org/10.1103/PhysRevB.72.184425
36. Vizhi, R.E., Rajan, R.: Structural, optical and room temperature magnetic properties of sol–gel synthesized (Co, Fe) co-doped SnO2 nanoparticles. J. Cryst. Growth **584**, 126565 (2022). https://doi.org/10.1016/j.jcrysgro.2022.126565
37. Banerjee, S., Tyagi, A.K.: Functional Materials: Preparation. Elsevier, Processing and Applications (2011)
38. Gaj, J., Kossut, J.: Introduction to the Physics of Diluted Magnetic Semiconductors. Springer, Berlin Heidelberg, Berlin, Heidelberg (2010)
39. Kharisov, B.I., Kharissova, O.V.: Radiation Synthesis of Materials and Compounds. CRC Press (2016)
40. Miglio, L., Montalenti, F.: Silicon-Germanium (SiGe) Nanostructures: Production, Properties, and Applications in Electronics. Woodhead Publishing, UK (2011)
41. Pohm, A.V., Comstock, C.S., Hurst, A.T.: Quadrupled nondestructive outputs from magnetoresistive memory cells using reversed word fields. J. Appl. Phys. **67**, 4881–4883 (1990). https://doi.org/10.1063/1.344766
42. Johnson, M., Bennett, B.R., Yang, M.J., Miller, M.M., Shanabrook, B.V.: Hybrid ferromagnet-semiconductor gates for nonvolatile memory. In: Seventh Biennial IEEE International Nonvolatile Memory Technology Conference. Proceedings (Cat. No.98EX141). pp. 78–83. IEEE (1998)
43. Engel, B.N., Akerman, J., Butcher, B., Dave, R.W., DeHerrera, M., Durlam, M., Grynkewich, G., Janesky, J., Pietambaram, S.V., Rizzo, N.D., Slaughter, J.M., Smith, K., Sun, J.J., Tehrani, S.: A 4-Mb toggle MRAM based on a novel bit and switching method. IEEE Trans. Magn. **41**, 132–136 (2005). https://doi.org/10.1109/TMAG.2004.840847
44. Datta, S., Das, B.: Electronic analog of the electro-optic modulator. Appl. Phys. Lett. **56**, 665–667 (1990). https://doi.org/10.1063/1.102730